

1 **Synopsis**

2

3 Bioinspired polyester elastomers synthesized from glycerol and tomato agrowaste, through a catalyst-
4 and solvent-free process display new and tunable properties.

5

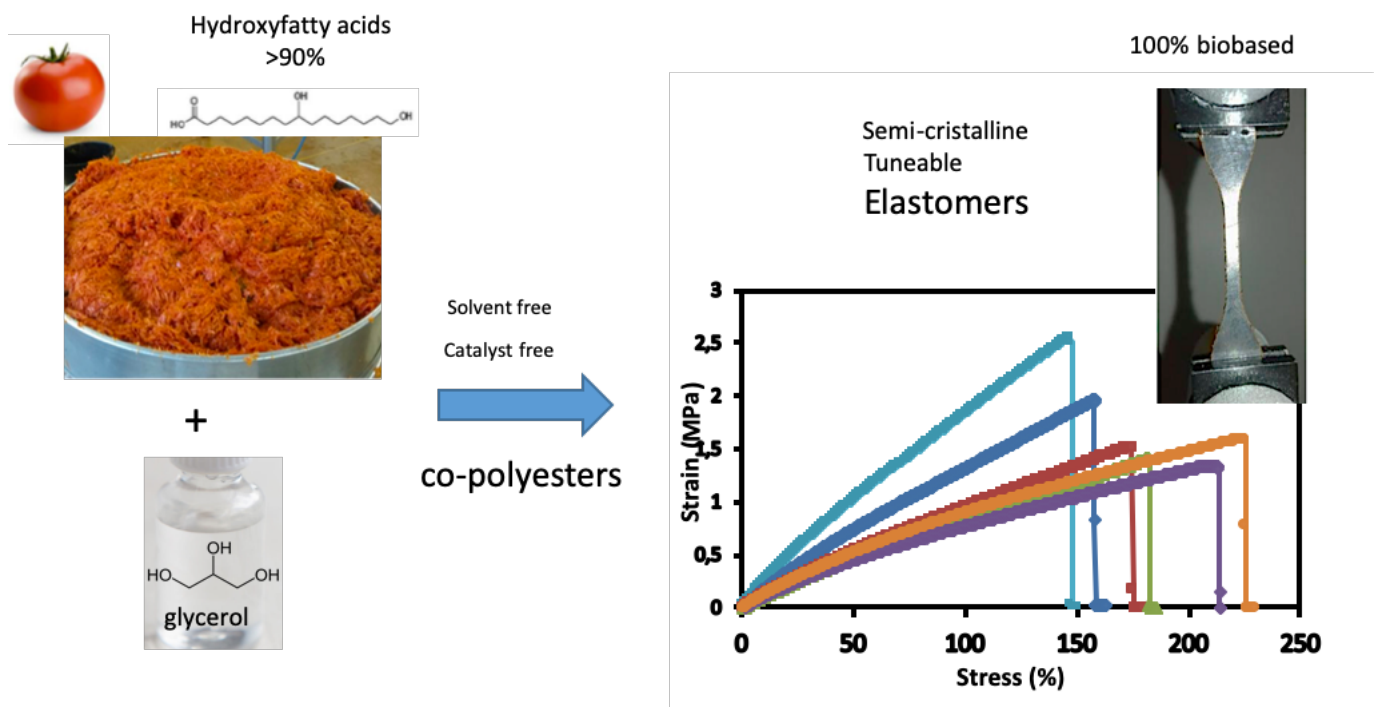
6 **Graphical abstract**

7

8

9

10



11

12

13

14

15 **Co-polyesters of hydroxy-fatty acids extracted from tomato peel agro-wastes and glycerol with tunable**
16 **mechanical, thermal and barrier properties**

17

18

19 Mathilde Marc[†], Regis Risani[†], Eric Desnoes[†], Xavier Falourd^{†,¶}, Bruno Pontoire[†], Rúben Rodrigues[&], Rita
20 Escórcio[&], Ana Paula Batista[‡], Romain Valentin[§], Nathalie Gontard[‡], Cristina Silva Pereira[&], Christelle
21 Lopez[†], Eric Leroy[‡], Denis Lourdin[†], Didier Marion[†], Bénédicte Bakan^{†*}.

22

23

24 [†] Biopolymers Interactions Assemblies Research Unit 1268 (BIA), INRAE, Rue de la Géraudière, 44316,
25 Nantes, France

26 [‡] Agropolymers Engineering and Emerging Technologies Joint Research Unit 1208 (IATE), INRAE-CIRAD-
27 SupAgro-University of Montpellier, 2 place Viala, Montpellier, 34000, France

28 [§] Agro-Industrial Chemistry Joint Research Unit 1010 (LCA), INRAE-INP-ENSIACET, 4 Allée Emile Monso,
29 Toulouse, 31000, France

30 [¶] Biopolymers and Structural Biology platform (BIBS), BIA research unit, INRAE, rue de la Géraudière,
31 Nantes, 44300, France

32 [‡] Université de Nantes. Oniris. CNRS. GEPEA. UMR 6144 44600 Saint Nazaire, France.

33 [&] Instituto de Tecnologia Química e Biológica António Xavier, Universidade Nova de Lisboa (ITQB NOVA),
34 Av. da República, Oeiras, 2780-157, Portugal.

35

36 *corresponding author: benedicte.bakan@inrae.fr

37

38 **Abstract**

39

40

41 By mimicking the cutin natural polyester networks of plant cuticles, we produced hydrophobic elastomers
42 by a sustainable process, i.e., using a catalyst- and solvent-free polycondensation of glycerol and hydroxy-
43 fatty acids, two by-products of the agro-food industry. The hydroxy-fatty acid fraction was obtained by
44 alkaline hydrolysis in ethanol of peels from industrial tomato pomaces. This industrial-like fatty acid
45 fraction contained more than 90% wt. of 9(10)-16 dihydroxyhexadecanoic acid (diOHC16). The co-
46 polyesters were designed by increasing the ratio of esterified glycerol/diOHC16 in a range observed in
47 plant cutins (up to 6% wt.). Their structure and functional properties (thermal, mechanical, gas
48 permeability, interaction with bacterial cells) were characterized. Increasing the glycerol contents induced
49 a significant decrease in the reticulation degree of the polyesters and the formation of crystalline domains
50 with an hexagonal organization. These structural modifications were related to a marked increase of
51 elastomeric extensibility (up to 217%). While water vapor permeability was not impacted, the increase of
52 glycerol content induced a significant decrease of oxygen permeability. None of the polyesters displayed
53 biocide activity, but an increase of glycerol content significantly reduced the adhesion of bacterial cells,
54 potentially giving rise to antifouling applications. Finally, the increasing content of free hydroxyl groups of
55 the co-polyesters offer opportunities of grafting and covalent substitution for tailored functionalization.

56

57

58

59

60

61 **Keywords**

62

63 Plant cuticle, biomimetic, cutin polyester, hydroxy-fatty acid, glycerol, semi-crystalline elastomer

64

65 **Introduction**

66 To face terrestrial life colonization, plants have developed a hydrophobic barrier, the cuticle, that covers
67 the surface of every aerial organs. This ubiquitous interface between the plant and its environment, fulfils
68 multiple crucial functions such as mechanical supports against wounding and cracks, control of non-
69 stomatal water loss and permeation of gases¹.

70 The main biopolymer of this complex hydrophobic assembly is the cutin polyester, that is essential
71 for the functional properties of the plant cuticle^{2, 3}. Cutin is insoluble due to its polyester network
72 architecture. It can be depolymerized mainly into a variety of long chain hydroxy-fatty acids building blocks.
73 Each of these carboxylic acid monomers contains 16 and-or 18 carbon atoms and one to three hydroxyl
74 groups. Interestingly, the tomato fruit peels concentrate high amount of cutin, whose monomer
75 composition is strikingly homogenous, with more than 80% by weight consisting of 9(10)-16
76 dihydroxyhexadecanoic acid (diOHC16). These ω -hydroxylated molecule carrying midchain functionalities,
77 present high interfacial properties ⁴, but constitutes also a unique opportunity for the development of
78 innovative biosourced polymer materials from depolymerized tomato cutin feedstock ⁵. Reaching this
79 innovation would address the important landmarks set by the United Nations sustainable development
80 goals because tomato cutin is a readily available residue of the tomato processing industries. Tomato
81 wastes, i.e., pomaces, are mainly composed of peels and seeds. 44 MT of tomato fruit are processed
82 worldwide, to make derived tomato products (e.g., purees, juice, sauces) generating nearly 1.5 MT of
83 animal feed and production of biogas whereas their transformation for development of new materials,
84 from bioplastic to high-functional value products remains largely overlooked ⁶. Peels and seeds can be
85 easily separated and dried, directly in the factory, and the hydroxy-fatty acids can be easily extracted from
86 the cutin of tomato peels ⁷.

87 Furthermore, glycerol, a main by-product of the biodiesel and oil industries ⁸, has been identified
88 as a potentially influent minor component in tomato cutin. Esterified glycerol has been evidenced in the
89 cutin polyester network structure ⁹ and typically represents only 0.6 to 0.7 % wt. of the cutin monomers
90 obtained by depolymerization (Philippe et al 2016). In addition, we have recently highlighted that the ratio
91 of the glycerol to hydroxy-fatty acid can be modulated in tomato fruit. Indeed, in tomato fruit mutants
92 affected in a cutin synthase (CUS1), an enzyme involved in the cutin biosynthesis, a 60% reduction in cutin
93 deposition was induced without any significant negative impact either on the fruit development or the

94 generation of cracks¹⁰. Looking at the cutin polyester structure, we observed a significant increase of ratio
95 of the glycerol to hydroxy-fatty acid. These results obtained with the mutants suggested that the inclusion
96 of co-polymerized glycerol in the tomato cutin network could be involved in the mechanical adaptation of
97 the fruit cuticle, in particular in the modulation of its extensibility. This is especially essential for resistance
98 to turgor pressure during fruit growth and environmental constraints to prevent fruit from cracking, a
99 phenomenon responsible for major crop losses¹². Taking inspiration from nature, our leading hypothesis
100 is that we can produce tunable bio-based co-polyesters that mimic potential adaptive events of cutin
101 simply by playing on the glycerol/diOHC16 ratio.

102 Hereinafter, we describe a solvent- and catalyst-free polymerization process to generate co-
103 polyesters elastomers from two diOHC16 and glycerol, two readily available and renewable biological
104 resources. Tuning of the ratio of esterified glycerol to diOHC16 in a range similar to what it is observed in
105 plant cutin effectively results in the modulation of the structure (amorphous or semi-crystalline), the
106 properties (mechanical, thermal and barrier properties) of the ensuing co-polyesters.

107
108

109 **Experimental Section**

110

111 **Materials**

112 Glycerol (99 % purity) and all other chemical ACS reagents were from Sigma-Aldrich (USA). The analytical
113 grade solvents were obtained from Carlo Erba (Val de Reuil, France). The 16-10(9)-hydroxy-hexadecanoic
114 acid enriched hydroxy-fatty acid fraction (referred as “diOHC16” in the manuscript) was extracted from
115 industrial tomato pomaces provided by the “Conserveries de Bergerac” (UNIPROLEDI, Bergerac, France).
116 The peels and seeds of the pomaces were separated by decantation in a water tank. The floating peels
117 were recovered, their water excess was squeezed out and then dried at room temperature. Dried peels
118 (1kg) were grounded and dewaxed under reflux of acetone: ethanol 1:1 (v:v) in a Soxhlet extractor and
119 then dried in a fume hood. Cutin depolymerization was conducted at room temperature in 5% (wt.) KOH
120 in ethanol 95%. After filtration on a Buchner funnel, about 90% of the filtrate was evaporated under
121 vacuum and replaced by water. Hydroxy-fatty acids were precipitated by adjusting pH at 3.5 with
122 concentrated HCl. The hydroxy-fatty acid precipitate was extensively washed with water, and finally
123 freeze-dried.

124 The purity of the fatty acids was determined after phase partitioning in CHCl₃/CH₃OH/H₂O 8:4:3
125 (v:v). The lower chloroform-rich phase containing only lipophilic compounds, mainly fatty acids and some
126 pigments, was recovered, evaporated under vacuum and weighed. The cutin monomer batches contains
127 98 ± 0.5% of lipophilic compounds. The fatty acid composition of the lipophilic fraction was determined by
128 gas chromatography coupled to a mass spectrometer as previously described ¹³. A 60% yield of hydroxy-
129 fatty acids was obtained and the same batch of 500g of diOHC16 extract was used in the study. This batch
130 was dark-red colored due to the remaining pigments and consisted of ~90 % diOHC16 (**Supplemental Table**
131 **1**).

132

133 **Preparation of the cutin-like co-polyesters films**

134 Co-polyesters films were produced by a solvent-free and catalyst-free polycondensation. We developed a
135 polymerization process in order to minimize the non-esterified glycerol within the copolyester films.
136 Preparation with different weight ratio of diOHC16/ Glycerol (1.8g diOHC16 for PG0.4 ; 1.71g diOHC16/90
137 mg glycerol for PG2.3; 1.62g diOHC16/180 mg glycerol for PG3.9; 1.53g diOHC16/ 270 mg glycerol for
138 PG4.8 ; 1.44g diOHC16/ 360 mg glycerol for PG5.2 and 1.35 g of diOHC16/ 450 mg glycerol for PG6.2
139 respectively) were put in Teflon molds (5 cm x cm) with a thickness of about 0.7-1 mm. The nomenclature
140 of the co-polyesters refers to the glycerol weight ratio comprised within the co-polyester at the end of the
141 process (**Table 1**). Bulk poly-condensation was then conducted for 24h at 150°C in an oven (VaccuTherm,
142 ThermoFisher, USA). In order to avoid bubbles and to minimize the presence of residual free glycerol, i.e.,
143 non-esterified, in the final material a 400mbar vacuum was applied during the first 2h of the
144 polycondensation process. After 24h, the polymers were rapidly cooled on ice and stored at room
145 temperature. Samples of the ensuing films were immersed under agitation in various solvents of diOHC16
146 and/or of glycerol, i.e., water, ethanol and chloroform 16h at room temperature to assess their solubility.

147

148 **Structural characterization of the cutin-like co-polyester films**

149 Attenuated total reflectance Fourier-transform infrared spectroscopy (ATR-FTIR) spectra (200 scans) were
150 recorded at a resolution of 2 cm⁻¹ on a Nicolet Magna IR 550 spectrometer equipped with a liquid nitrogen
151 cooled mercury-cadmium-telluride detector. The instrument was continuously purged with dry air.
152 Spectra of co-polyester films were obtained by attenuated total reflection (ATR) using

153 a single reflection accessory fitted with a thermostated diamond crystal with a 45° angle of light incidence.
154 All spectra (3 per co-polyester) were acquired in the 4000 to 700 cm⁻¹ range at 4cm⁻¹ resolution and
155 accumulating 30 scans.

156 ¹³C solid state NMR (CP-MAS NMR) was carried out on a Bruker AvanceIII-400 MHz spectrometer
157 operating at 100.61 MHz for ¹³C, equipped with a double-resonance H/X CP-MAS 4-mm probe for CP-MAS
158 (cross-polarization magic-angle-spinning) solid-state experiments. Sixty mg of the co-polyester films were
159 put packed into 4 mm zirconia rotors. The samples were spun at 12,000 Hz at room temperature. CP-MAS
160 spectra were acquired with a contact time of 1 ms, a recycling delay of 10 s and over accumulation of 2048
161 scans. The carbonyl carbon was set to 176.03 ppm through external glycine calibration. NMR spectra
162 deconvolution was performed using the PeakFit® software (Systat Software, Inc., USA).

163 X-Ray Diffraction analysis was performed on a Bruker-AXS D8 Discover diffractometer. The X-ray
164 beam was produced in a sealed copper tube at 40 kV and 40 mA. The 500-µm beam with a CuKα1
165 wavelength (1.5405 Å) was collimated and parallelized using two crossed-coupled Göbel mirrors. The X-
166 ray diffraction data were collected using a Vantec500 two-dimensional detector, previously calibrated with
167 silver behenate, in the 2.θ-range: 3-70°. The samples are placed perpendicular to the X-ray beam. Recorded
168 diffractograms $I = f(2\theta)$ were normalized to remove the influence of thickness variation among the
169 samples. Temperature kinetics were performed using Linkam's HFS91 stage. The samples were placed in a
170 mica window cell. The detector was positioned at a focusing distance of 8.6 cm from the sample surface.
171 It was in direct beam position. The heating kinetic applied to the sample was 3°C.min⁻¹ from 20°C to 100°C.
172

173 **Chemical characterization of the cutin-like co-polyester films**

174 Free glycerol was extracted from polymers (5mg in 1 mL of CH₃OH), overnight at room temperature.
175 Esterified glycerol was released from polymers by mild methanolysis using a modified procedure ⁹. Isolated
176 pieces of the co-polyester films were stirred at room temperature in a mixture of 50mM sodium methoxide
177 in dry methanol with the internal standard 1,2,3-butanetriol ¹⁴. Free and esterified glycerol extracts were
178 dried with a nitrogen flow, and analyzed by GC-MS and GC FID. For the quantification of the cutin hydroxy-
179 fatty acids, the co-polyesters were depolymerized through methanolysis according to a described
180 procedure during 6h until complete depolymerization. The depolymerized hydroxy-fatty acids were
181 silylated with 1% BSTFA/TMCS and analyzed by GC-MS and GC-FID as previously described ¹¹.

182 Free OH groups were derivatized by benzyl-etherification resistant to alkaline depolymerization,
183 according to an established method ¹¹. Briefly, co-polyesters (3mg) were mixed at 90°C in a screw-capped
184 glass tube for 24h with 15mg of 2-benzyloxy-1-methylpyridinium triflate and 1.68 mg of magnesium oxide
185 in 1mL of trifluorotoluene. The samples were then extensively washed with CH₂Cl₂ and dried before
186 depolymerization and cutin monomer analysis. GC-FID surface response of the labelled diOHC16 (either in
187 midchain position or in ω-position) were compared between the different co-polyesters and were
188 expressed as equivalent of heptadecanoic acid, as external standard.

189

190 **Thermal and mechanical properties of the cutin-like co-polyester films**

191 Differential Scanning Calorimetry (DSC) was performed on a DSC Q100 (TA Instruments, New Castle, DE,
192 USA). The DSC instrument was calibrated with an indium standard. Analyses were made with 2–5mg of
193 samples, using hermetically-sealed aluminium pans. An empty pan was used as a reference. Samples were
194 cooled from 20°C to –50°C and heated at 3°C.min⁻¹ until 80°C. The Glass transition temperature (T_g) of the
195 co-polyesters was defined at the midpoint of heat capacity change on the thermograms recorded on the
196 first scan. The melting temperature was determined at the maximum of the peak.

197 Dynamic Mechanical Thermal Analysis (DMTA) was performed on a DMTA MKIV (Rheometric
198 Scientific, US). Rectangular specimens (20 mm ×4 mm) were cut from the films and thickness of about 0.7-
199 1 mm was precisely measured with a micrometer. The samples were analyzed in the tensile mode at the
200 frequency of 1 Hz with strain amplitude of 0.1%. To keep the samples taut a static force superior by 10%
201 to the dynamic force was applied to the sample. A scanning rate of 3°C min⁻¹ from -50°C to 80 °C was used.
202 Each sample was analyzed in duplicate.

203 Tensile test of the films was carried out using MTS Synergie 100 (MTS Systems Corporation, USA).
204 The film samples were cut into a dog-bone shape. The test was performed using a cross-head speed of 10
205 mm/min. The reported results, including Young's modulus, ultimate strength and elongation at break,
206 were the average values of five specimens. The standard deviations are indicated in **Table 1**.

207

208 **Barrier properties of the cutin-like co-polyester films**

209 Water permeances of the co-polyesters were determined at 25°C and under 100% relative humidity
210 gradient using transpiration chambers as previously described ^{11, 15}. Typically, co-polyesters (5 replicates)
211 were mounted on the top of the transpiration chamber with a 0.6 cm diameter hole, subsequently filled

212 with 300 μL of deionized water, inverted and placed in a desiccator filled with a desiccant. Water transfer
213 across the co-polyesters samples was determined by gravimetric analysis of the transpiration chamber
214 every 8h during 4 days. Water permeance (P) was calculated as the ratio $P=F/A.\Delta c$, where F (Flow rate of
215 water) is determined as the slope of water transfer across the samples (in $\text{g}.\text{s}^{-1}$), A (in m^2) is the area across
216 which transport has occurred, and Δc (in $\text{g}.\text{m}^{-3}$) is the water gradient driving force.

217 The oxygen permeability of co-polyesters was determined in triplicate at 23°C and 0% relative
218 humidity through an isostatic and dynamic method using gas-phase chromatography as previously
219 described¹⁶. The film samples (4 cm diameter) were placed inside sealed stainless-steel permeability cells.
220 The lower chamber was continuously spread by a $5 \text{ mL}.\text{min}^{-1}$ flux of permeant gas (O_2), and the upper
221 chambers by the same flux of vector gas (helium), thus applying a permanent O_2 partial pressure
222 difference. The permeability cells were coupled to a gas chromatograph with thermal conductivity detector
223 (GC-TCD, Agilent 7890A, USA), equipped with an automatic valve to online analyze the evolution with time
224 of O_2 gas concentration in the upper chamber. The GC-TCD was equipped with two capillary columns -
225 PoraPlot U ($25 \text{ m} \times 0.530 \text{ mm id}$, Agilent) and HP Molesieve ($30 \text{ m} \times 0.535 \text{ mm id}$, Agilent) – able to separate
226 O_2 , CO_2 and N_2 . Data were collected and processed using the ChemStation OpenLab Software (Agilent) and
227 SRA Prochem interface (SRA Instruments). The O_2 permeability, P_{O_2} ($\text{mol}.\text{m}^{-1}.\text{s}^{-1}.\text{Pa}^{-1}$), of the film samples
228 was calculated as follows:

$$229 \quad P_{\text{O}_2} = \frac{J \times e}{A \times \Delta P} \quad (\text{equation1})$$

230 Where: J ($\text{mol}.\text{s}^{-1}$) is the flux of gas that pass through the film, e is the film thickness (m), A is the permeation
231 area (m^2) and ΔP is the O_2 pressure differential between the upper and lower chambers of the cell (Pa).

232

233 **Microbiological analyses**

234 *S. aureus* NCTC8325 and *E. coli* TOP 10 cells (10^5 cells. mL^{-1}) in Mueller-Hinton broth (MHB) medium were
235 exposed for 24h to 0.5 cm^2 of polyester films (*ca.* 10 to $20 \text{ mg}.\text{mL}^{-1}$) at 37°C , under orbital agitation (100
236 rpm). Upon incubation, the cellular morphology and the viability of the bacterial cells were visualized by
237 light and fluorescent microscopy, respectively, using a Leica DM6000 B microscope equipped with an iXon
238 EM+ 885 EMCCD camera (Andor Technology®). The fluorescent dye propidium iodide (PI) was used for
239 labelling the dead cells (red fluorescence). Negative controls, i.e., bacteria growing in media devoid of
240 cutin-like co-polyester films, were also carried out. Films from each tested condition were also collected

241 to scan for the presence of bacterial cells on the film's surface. All assays were done in triplicate. The films
242 were first washed with phosphate buffered saline (PBS) to remove non-adherent bacteria, subsequently
243 fixed with glutaraldehyde 2.5% (v/v) during 10 min. After 10 min, samples were rinsed with distilled water
244 and dehydrated with aqueous solutions with increasing concentration of ethanol (ranging from 70 to
245 100%). Scanning electron microscopy (SEM) (microscope JEOL JSM-7001F, with an accelerating voltage set
246 to 15 kV) was used to scan the co-polyester film's surfaces. All samples were coated with gold before
247 analysis.

248

249

250 **Results and Discussion**

251 **Sustainable production of dark black colored insoluble co-polyesters with different ratio of esterified-** 252 **glycerol**

253 The cutin-like polyesters were manufactured to meet green chemistry and sustainability criteria. Indeed,
254 they were prepared through a catalyst- and solvent-free process using hydroxy-fatty acids and glycerol
255 from renewable resources, i.e., agro-wastes and by-products of the tomato and oilseed processing
256 industries. The hydroxy-fatty acids were extracted following two major biorefinery steps i) fractionation of
257 industrial wastes, i.e., tomato pomaces, into seeds and peels and ii) the processing of peels to recover the
258 hydroxy-fatty acids of the tomato cutin polyester. In both steps, green solvents were used, water and
259 ethanol, which can be recycled to improve the sustainability of the process. The dewaxing step performed
260 in this work, to limit the molecular complexity of this study, could be by-passed, since waxes account for
261 less than 5% (wt.) of tomato cuticles¹⁰. In contrast with previous studies, the extraction of fatty acids from
262 peels, instead of raw pomaces provided a fatty acid fraction with a higher diOHC16 content (90% instead
263 of 45%)¹⁷. Interestingly, the alkaline hydrolysis in ethanol at room temperature gave rise to a high fatty
264 acid yield (around 60% wt. of dry peels), instead of around 15% wt. for hot aqueous alkaline hydrolysis¹⁸
265 thereby strengthening the sustainability of the process. The tomato seeds, a major by-products of pomace
266 biorefinery, can be used for animal feed and human food due to the good nutritional quality of their
267 protein, oil and fiber fractions, or for the production of biogas¹⁹. Finally, a similar sustainable processing
268 of tomato pomaces was recently developed at the industrial scale for the internal coating of food cans
269 (<https://www.tomapaint.com/>).

270

271

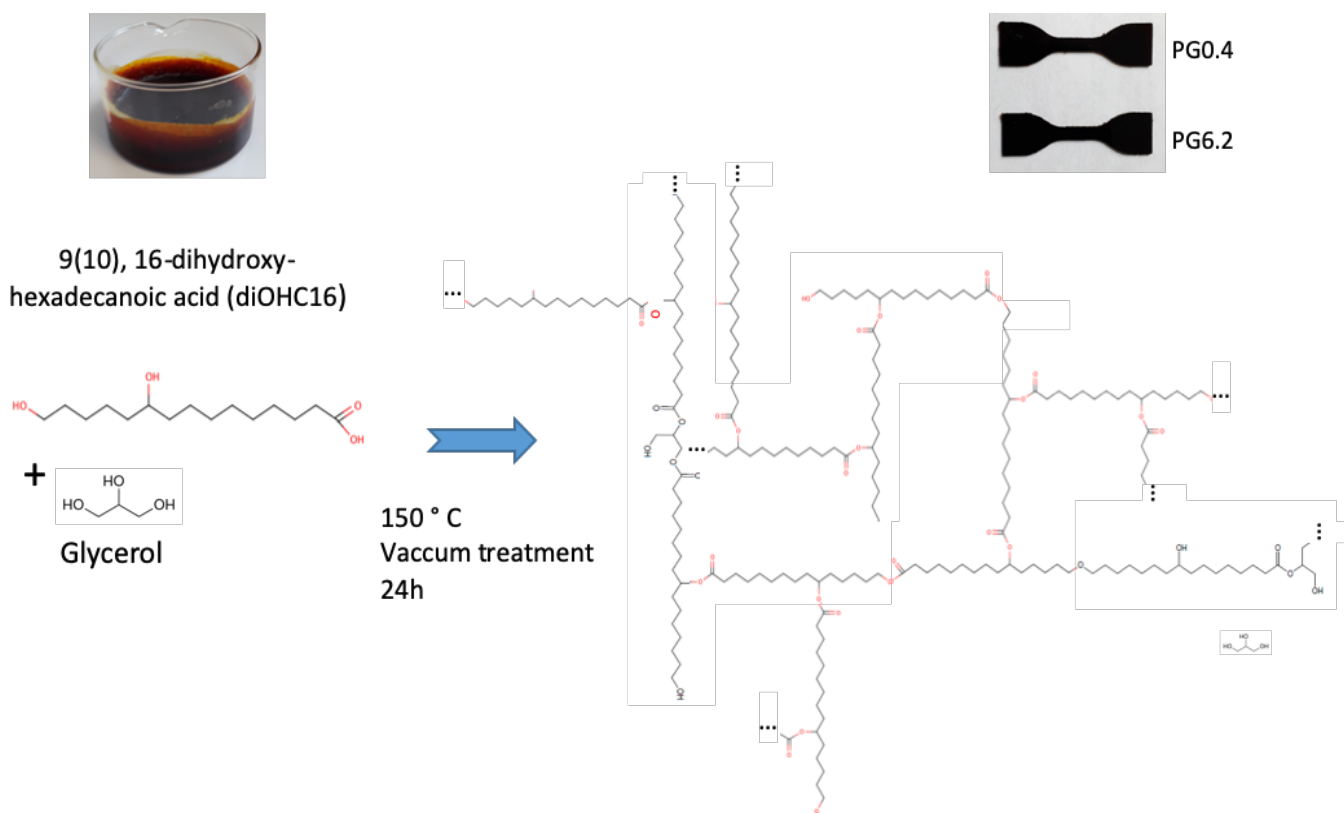


Figure 1 – Schematic representation of the solvent- and catalyze-free polycondensation of tomato cutin hydroxyfatty acid and glycerol

272

273

274

275

276

277

278 The cutin-like co-polyesters formed by polycondensation of the diOHC16-rich hydroxy-fatty acid
279 extract and glycerol (**Figure 1**) displayed a dark brown color. All the polyester films were almost insoluble
280 in water, ethanol and chloroform (**Table 1**). This low solubility of the co-polyesters is therefore ascribed to
281 the formation of cross-linked networks. Minor hydroxy-fatty acids including some dioic acids, as well as
282 phenolic compounds (**supplemental Table 1**) present in the diOHC16 extract, are also insolubilized during
283 polymerization and therefore, are also involved in the formation of the polymer network. In the
284 amorphous polymers produced from whole tomato pomace, it has been proposed that impurities and their

285 oxidation could lead to the formation of additional acid functions during the polymerization, strengthening
286 the formation of cross-linkages ⁷. In our case, similar oxidation processes should occur as evidenced by the
287 darkening that occurs during the polymerization process (**Figure 1**). Although these minor compounds and-
288 or their oxidation products cannot be ignored, all other things being equal, the main variable of this study
289 was the glycerol content. Accordingly, we can follow the modulating effect of glycerol on the properties of
290 the co-polyesters produced from the fatty acid extract from peels provided from tomato pomaces, in line
291 with a vision of a sustainable cutin-inspired chemistry.

292 To fulfill this objective, in the aim to monitor the effect of glycerol addition onto the cutin-*like* co-
293 polyesters properties, materials containing different amounts of esterified glycerol were produced. After
294 the poly-condensation reaction, the added glycerol can be (i) free, i.e., non-esterified, acting as an external
295 plasticizer, or (ii) esterified, constituting a polyester monomer. Determination of free and esterified
296 glycerol contents revealed that more than 95% of the glycerol was esterified (**Table 1**).

W water, CF chloroform, Et Ethanol

Table 1 Composition, chemical, thermal and mechanical characterization of the cutin-inspired co-polyesters

Sample	Chemical characterisation						DSC					DMTA			Mechanical test		
	glycerol total (%wt)	esterified glycerol (% wt)	free glycerol (% wt)	insoluble fraction (%) W	insoluble fraction (%) CF	insoluble fraction (%) Et	Glass transition temperature (°C)	Melting temperature 1 (°C)	Melting Enthalpy (J/g)	Melting temperature 2 (°C)	Melting Enthalpy (J/g)	Mechanical relaxation temperature (°C)	Storage Modulus at 50°C (MPa)	Breaking stress (MPa)	Strain at break (%)	Young's modulus (Mpa)	
PG0.4	0.43 ± 0.24	0.38 ± 0.21	0.05 ± 0.04	100	100	98	-8.7	-	-	-	-	8.6	5.867	2.1 ± 0.5	124.0 ± 24.5	2.29 ± 0.05	
PG2.3	2.27 ± 0.31	2.17 ± 0.32	0.10 ± 0.03	99	100	98	-13.1	-	-	-	-	5.4	5.035	2.0 ± 0.2	155 ± 12.7	1.74 ± 0.06	
PG3.9	3.93 ± 0.34	3.75 ± 0.31	0.18 ± 0.05	99	99	94	-15.7	-	39.7	0.07	-	3.2	4.058	1.7 ± 0.2	180.7 ± 10.3	1.26 ± 0.2	
PG4.8	4.80 ± 0.82	4.57 ± 0.80	0.23 ± 0.15	99	97	95	-17.0	17.9	41.6	0.32	2.60	1.9	1.408	1.4 ± 0.1	178.4 ± 8.6	1.11 ± 0.03	
PG5.2	5.20 ± 0.31	4.87 ± 0.5	0.32 ± 0.2	99	94	91	-20.4	16.8	41.2	2.04	7.96	0.9	1.521	1.3 ± 0.1	197.3 ± 21.1	1.10 ± 0.01	
PG6.2	6.18 ± 0.39	5.89 ± 0.45	0.29 ± 0.1	100	88	80	-18.5	18.3	41.6	0.59	9.05	0.2	1.589	1.5 ± 0.1	217.6 ± 14.2	1.19 ± 0.08	

298 **A gradual increase of the glycerol content induces a decrease in the branching of the co-polyester films**
299 The co-polyesters containing the lowest (PG0.4) and the highest (PG6.2) levels of esterified glycerol were
300 characterized by ATR- FTIR and ^{13}C NMR (**Figure 2**). ATR-FTIR clearly indicated the formation of esters
301 bonds in these co-polyesters. Indeed, we observed the characteristic shift of the carbonyl band from 1705
302 cm^{-1} , assigned to the carboxylic acid, to the 1733 cm^{-1} band assigned to the esterified carbonyl²⁰. In
303 addition, the 1715 cm^{-1} band assigned to the ester bond involved in hydrogen bonding were also
304 evidenced, as previously observed in tomato cutin ¹⁰. In our present co-polyesters, the hydrogen bonds
305 could involve the free hydroxyl groups either from the hydroxy-fatty acids and/or from the esterified
306 glycerol. Besides, the 1171 cm^{-1} band assigned to the stretching vibration of the C-O-C ester bond was
307 observed in all co-polyesters. Likewise, the ^{13}C C-MAS (**Figure 2B**) data confirmed the formation of esters,
308 evidenced by a single broad peak at 173 ppm and by the peak at 64 ppm, which is assigned to primary
309 esters ¹⁷. In addition, no significant free fatty acid signals were evidenced at 178 ppm (-COOH) and at 35
310 ppm (-CH₂-COOH). Finally, the comparison of the surface ratio of the 33.7 ppm and 37 ppm peaks, assigned
311 to aliphatic carbons (-CH₂-CHOR-CH₂-) and (CH₂-CHOH-CH₂) respectively ²¹, indicated a decrease (40%) in
312 the esterification of the secondary hydroxyls of diOHC16 associated with the increase in the glycerol
313 content.

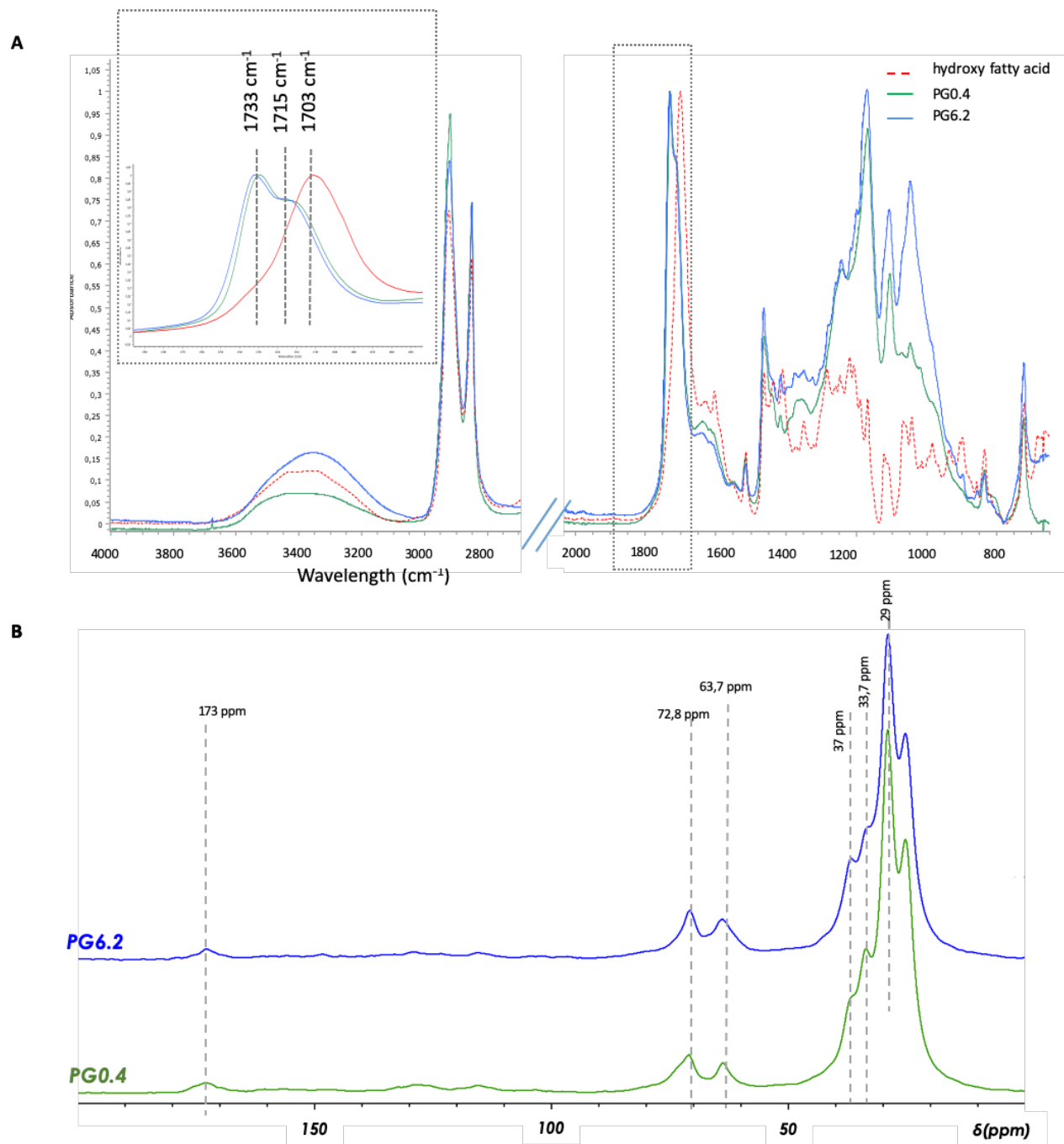


Figure 2- ATR-FTIR and NMR spectra of the cutin-like polyesters films

A . ATR-FTIR spectra of hydroxy-fatty acid (diOHC16) extracted from tomato cutin and the corresponding polymers with high (PG6.2) or low (PG0.4) glycerol. In inset, the magnification of the CO stretching bands at 1733 cm^{-1} and 1715 cm^{-1} are assigned respectively to ester group, and ester bond interacting by hydrogen bond whereas the band at 1703 cm^{-1} is assigned to carboxylic group.

B. Solid State ^{13}C CP-MAS NMR spectra of the polymers

315 The reticulation of the co-polyesters was further monitored by the chemical labelling of the free OH
316 groups by benzyl ether within the diOHC16-derived polyesters ¹¹ (Figure 3).

317

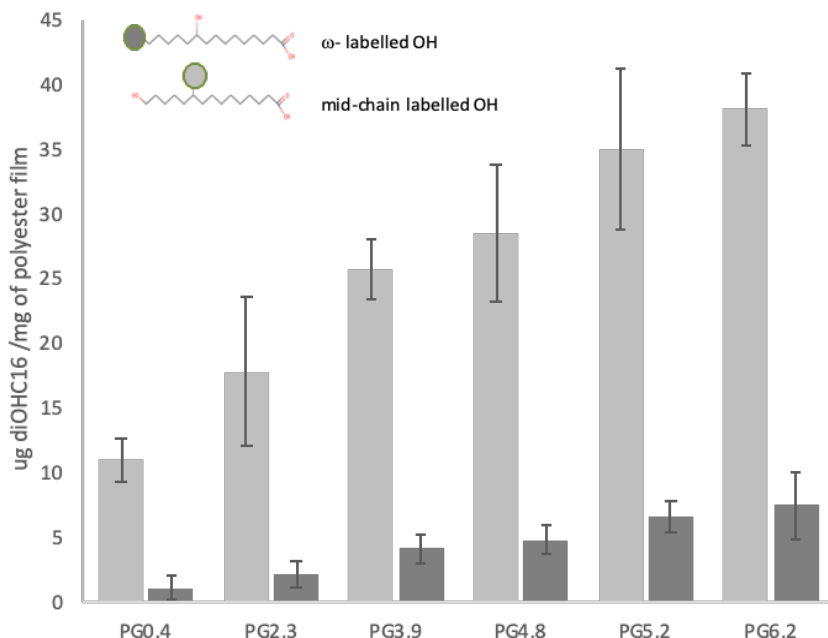


Figure 3. Relative proportion of free OH groups at the ω - and mid-chain position of the the diOHC16 in the co-polyester films.

Values are means of at least three replicates bars are standard deviations

318

319 According to the chemical structure of the diOHC16, both, linear and branched ester bonds, can be
320 formed in the co-polyesters. After complete depolymerization, the release of diOHC16 containing labeled
321 OH groups either in ω -position or in midchain-position was compared in the different co-polyesters. In
322 PG0.4, the ratio of labeled mid-chain OH/ ω -OH labeled in diOHC16 was around 9, which indicates that the
323 primary OH groups in the ω -position were preferentially esterified compared to the OH groups in the
324 midchain position. This result agrees with the NMR data (Figure 2B) and the previous studies of
325 polycondensation of polyhydroxylated fatty acids ²¹. A similar ratio was previously reported for tomato
326 fruit cutin ¹¹. Furthermore, taking PG0.4 as a reference, the gradual introduction of glycerol in the co-
327 polyesters resulted in a gradual increase (up to 3.5-fold) in the labeled OH groups, in particular in the
328 midchain position. These results indicate that the introduction of glycerol in the co-polyesters induced a
329 gradual decrease in the esterification of midchain hydroxyl groups involved in ester bonds and an increase
330 in the linear polymerization scheme within the co-polyesters.

331 **Glycerol content modulate the elastomer properties of the co-polyesters**

332

333 The thermal properties of all the produced co-polyesters were investigated by DSC on heating from -50°C

334 to 80°C at 3°C.min⁻¹. Characteristic thermograms are superimposed on the **Figure 4A**.

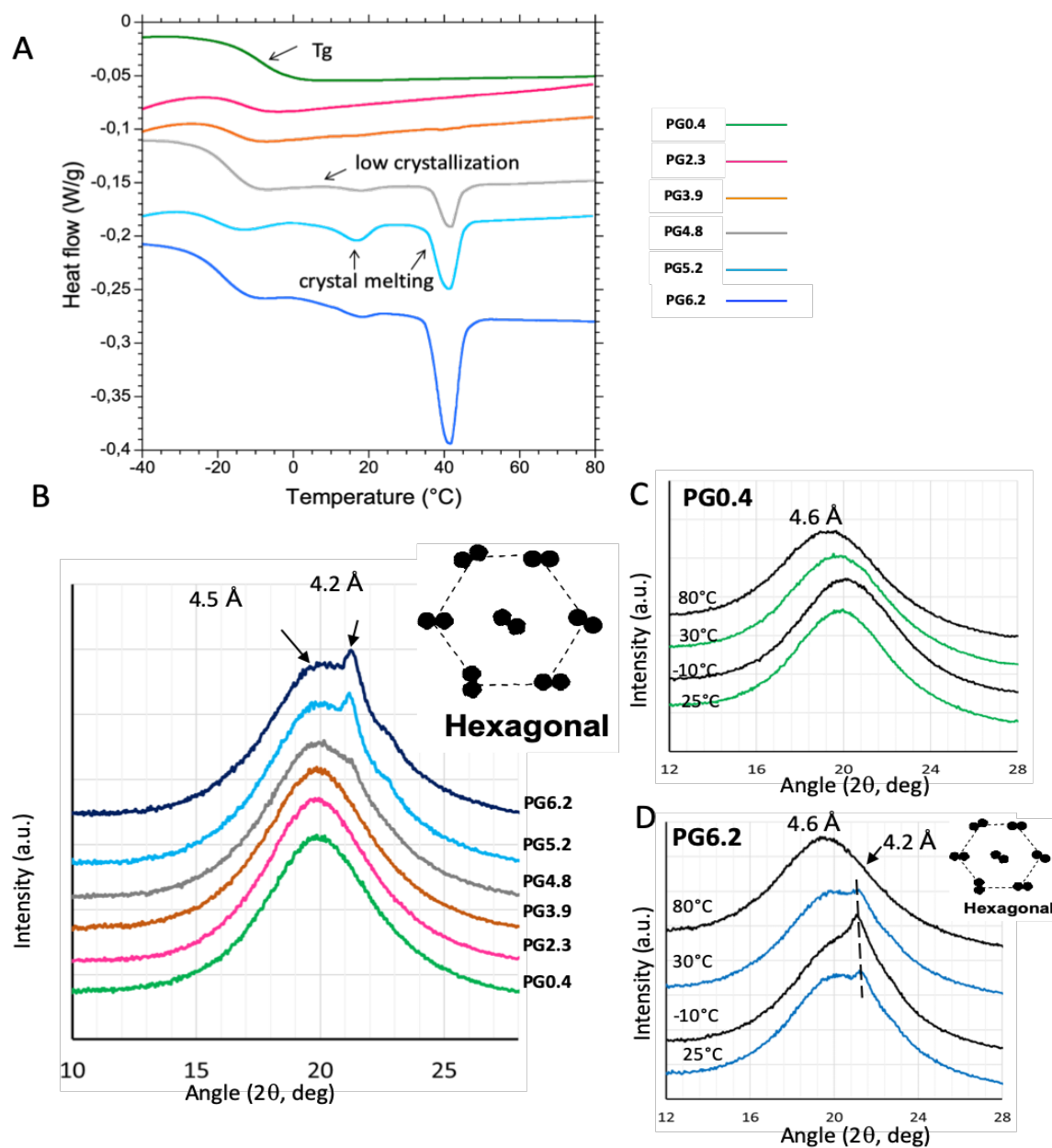


Figure 4. DSC and XRD analyses of the different cutin-like diOHC16-glycerol co-polyester films

A . DSC thermogram of the different co-polyesters containing increasing level of glycerol from 0.4 % wt (for PG0.4) to 6.2% wt (for PG6.2). **B** , XRD patterns of the different co-polyesters recorded at 25°C., XRD patterns recorded for PG0.4 (**C**) and PG6.2 (**D**) at different temperatures.

335

336 We checked that the cooling step at -50°C did not modify the crystallinity of the samples. The
337 thermograms of the co-polyesters exhibited various events as a function of the composition, i.e., the
338 amount of esterified glycerol in the samples. From -10°C to -20°C , the baseline fall was attributed to the
339 glass transition characterizing the amorphous phase of the co-polyesters. The glass transition
340 temperatures (T_g), determined at the midpoint of the baseline fall, were determined for each co-polyester
341 (**Table 1**). The T_g value recorded for the PG0.4 sample containing only traces of glycerol is -8.7°C , similar
342 to that measured on polyester catalyst- produced (-7°C) from hydroxy-fatty acids extracted from green
343 tomato cutin ²¹. Interestingly, the T_g significantly decreased from -8.7 to -20.4°C with the gradual
344 introduction of glycerol (up to 6.2% wt.) within the co-polyesters, suggesting that the mobility of the co-
345 polyester chains increased giving rise to a more relaxed structure. This result is consistent with the
346 observed reticulation pattern of the co-polyesters (**Figure 3**).

347 For the co-polyesters containing glycerol amounts lower than 4% wt. (PG0.4, PG2.3, PG3.9), the
348 DSC thermograms recorded on heating did not exhibit thermal events above 0°C (**Figure 4A**). However, for
349 the co-polyesters containing higher amounts of glycerol (PG4.8, PG5.2 and PG6.2), endothermic events
350 were recorded and related to the gradual incorporation of glycerol in the materials. Indeed, for these co-
351 polyesters two successive endothermic peaks were recorded around 17°C and 40°C . These endotherms
352 may correspond to structural reorganizations, and/or changes in the physical state of molecules in the co-
353 polyesters. The first peak (17°C), seems to be preceded by an exothermic peak, probably due to a low
354 crystallization event (**Figure 4A**), and exhibits a low enthalpy that could not be clearly related with glycerol
355 content (Table 1). The second endothermic peak (40°C) exhibits a higher enthalpy which increases with the
356 level of glycerol content (**Table 1**).

357 The X-ray diffraction experiments performed at 25°C showed at wide angles a bump centered at
358 $2\theta=19^{\circ}$ ($d=4.5 \text{ \AA}$), corresponding to the amorphous state of the co-polyesters (**Figure 4B**). In the co-
359 polyesters containing at least 5 % wt. of glycerol (PG5.2, PG6.2), a peak at $2\theta=21.2^{\circ}$ was recorded (**Figure**
360 **4B**). This peak corresponds to a repeat distance of 4.2 \AA between the acyl chains that is characteristic of
361 an hexagonal packing of acyl chains. This single peak constitutes the XRD signature of the formation of a
362 crystalline organization of the linear esterified acyl chains within the co-polyesters containing at least 5%
363 wt. glycerol. This XRD peak was superimposed to the bump centered at 4.5 \AA (**Figure 4B**), that corresponds
364 to the coexistence of crystalline and amorphous states within the co-polyesters. The presence of glycerol

365 in the samples, and the esterification occurring between the hydroxyl groups of glycerol (mainly in *sn-1*
366 and *sn-3* positions) and the carboxyl groups of the fatty acids induced a linear organization of the chains
367 or the formation of shorter chains. This spatial proximity between the linear and shorter co-polyester
368 chains may favor short-distance hydrophobic interactions between the acyl chains and result in a
369 crystalline organization with a hexagonal packing below the melting temperature of the fatty acids. In
370 absence of glycerol, the reticulation involves the hydroxyl groups both in midchain hydroxyl and ω -
371 positions. This prevents short-distance hydrophobic interactions between the linear chains formed by
372 primary esterification, hence avoiding the formation of a crystalline organization in the co-polyesters.

373 The thermotropic phase behavior of the co-polyesters formed with very low (PG0.4) or high (PG6.2)
374 amount of glycerol, were investigated by XRD at various temperatures ranging from -10°C to 80°C that
375 have been selected according to the DSC results (**Figure 4A**). In presence of very low glycerol content
376 (**Figure 4C**), the amorphous state of the polyester was characterized by a bump of RX diffusion, centered
377 in a mean value that was affected by the temperature. Increasing the temperature induced a shift toward
378 lower angle values corresponding to higher distances between the acyl chains associated with an increase
379 in the molecular mobility. In the presence of 6 % wt. of glycerol (**Figure 4D**), the XRD experiments were
380 conducted at 25°C, then the samples were cooled to -10°C, heated to 30°C (i.e., above the first endotherm)
381 and then finally to 80°C (i.e., above the second endotherm). The single peak at $2\theta=21.2^\circ$ (4.2 Å) was
382 recorded at 25°C, confirming the results previously obtained. Decreasing the temperature to -10°C
383 increased the intensity of the XRD peak at $2\theta=21.2^\circ$ related to a hexagonal phase and was interpreted as
384 an increase in the amount of the crystalline phase formed in the co-polyesters. On heating at 30°C, the
385 intensity of the XRD decreased. Increasing the temperature at 80°C, i.e., above the second endotherm
386 recorded by DSC and then above the melting point of the crystalline structures, induced the disappearance
387 of the XRD peak at $2\theta=21.2^\circ$ and to the recording of an XRD bump centered at 4.6 Å characteristic of acyl
388 chains in a melted state. These XRD experiments evidenced the temperature-dependent behavior of the
389 co-polyester, with presence of various amounts of hexagonal phase as a function of temperature.

390 The two endotherms revealed successively by DSC correspond to independent packing events of
391 the molecules both organized in an hexagonal form as revealed by XRD. The different melting
392 temperatures may correspond to packing of molecules with various compositions, e.g. chain length.

393 The thermo-mechanical behavior of all co-polyesters were analyzed by DMTA. **Figure 5A** shows the
 394 plot of the storage modulus (E') and the loss factor $\tan \delta$ of the co-polyesters.

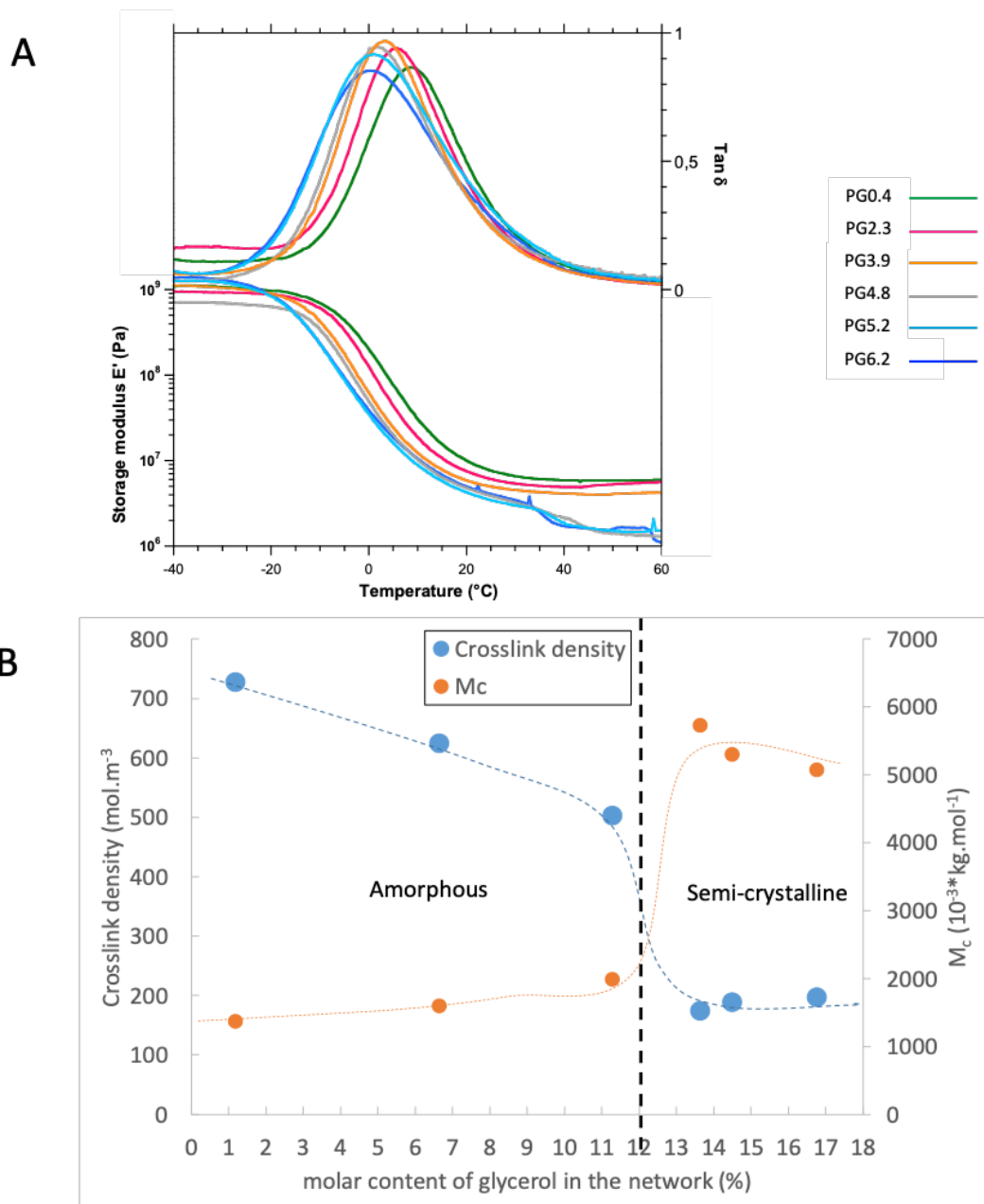


Figure 5 – DMA analysis of the cutin-like diOHC16-glycerol co-polyesters

A – Plot of the storage modulus (E') and the loss factor $\tan \delta$ of the co-polyesters with different level of esterified glycerol content.

B- Evolution of the crosslink density and the average mass between crosslinks as a function of the molar content of glycerol in the network. Dashed lines are just guides for the eyes.

396 For all samples, the large peak of $\tan \delta$ corresponds to the main mechanical relaxation α which is
397 associated to the calorimetric glass transition of the elastomer (transition from glassy to rubbery state).
398 The relaxation temperature from the glassy to the rubbery state ($T\alpha$), determined at the maximum of the
399 $\tan \delta$ curve, decreases from 8.6°C to 0.2°C when glycerol content increases (**Table 1**). In agreement with
400 the T_g values obtained by DSC analyses (**Table 1**) such depressor effect of glycerol on $T\alpha$ further
401 strengthens the impact of the glycerol on the properties of the cutin-like co-polyesters.

402 A second event appears on storage modulus which slightly fall in the temperature range 30-40°C
403 for the composition containing more than 4% (wt.) of glycerol (PG4.8, PG5.2, PG6.2) (**Figure 5A**). This
404 transition is attributed to the melting of the crystalline phase according to DSC and XRD results (**Figure 4**).
405 Finally, the plateau of storage modulus is reached at about 50°C with a value which decreases from 5.867
406 MPa to 1.589 MPa when glycerol content increases from 0.4 to 6% wt. (**Table 1**).

407
408 Since these values are typical of rubber elasticity, the Flory theory²² may be used to relate them to
409 the structure of the networks²³. Accordingly, the crosslink density ν (mole.m⁻³) is given by:

410
$$\nu = \frac{E}{3RT} \quad (\text{equation 2})$$

411 Where: R is the gas constant 8.32 J.mol⁻¹.K⁻¹, T is the temperature in Kelvin and E the elastic modulus at
412 small deformation.

413 Therefore, the average molecular mass M_c (kg.mol⁻¹) between crosslinks is:

414
$$M_c = \frac{3RT\rho}{E} \quad (\text{equation 3})$$

415 Where: ρ is the density of the material in Kg.m⁻³. In the present case, E corresponds to the plateau storage
416 modulus measured in DMTA at 50°C (T = 323 K). The density of the co-polyesters at this temperature could
417 not be measured. As a first approximation, we considered a constant density $\rho = 1000$ kg.m³ for the
418 calculations reported in **Table 2 and Figure 5B**.

	n	M _c (g/mol)	M _c /M ₀	Esterified molar glycerol content *
	(mol.m ⁻³)	(10 ⁻³ kg.mol ⁻¹)	-	mol %
PG 0.4	728	1374	5.1	1.2
PG 2.3	625	1601	5.9	6.64
PG 3.9	503	1987	7.4	11.3
PG 4.8	175	5726	21.2	13.6
PG 5.2	189	5301	19.6	14.5
PG 6.2	197	5074	18.8	16.8

* the molar content of glycerol in the networks given by

$$\text{esterified Glycerol (mol\%)} =$$

$$\frac{\frac{\text{esterified glycerol w\%}}{M_{\text{glycerol}}}}{\frac{\text{esterified glycerol w\%}}{M_{\text{glycerol}}} + \frac{(100 - \text{free glycerol w\%} - \text{esterified glycerol w\%})}{M_{\text{diOHC16}}}}$$

Table 2 : Macromolecular structure of the network predicted by the Flory theory

419

420

421 The elastomers PG0.4, PG2.3 and PG3.9 show the largest crosslink density values in the range of 500- to
 422 730 mol.m⁻³ associated to small values of M_c in the 1300-2000 g.mol⁻¹ range. Concurrently, much lower
 423 values of ν (175 to 200 mol.m⁻³) are obtained for samples PG4.8, PG5.2 and PG6.2, with higher values of
 424 M_c in the 5000-5700 g.mol⁻¹ range.

425 In a first approximation, the number of polymerized diOHC16 repeating units between crosslinks
 426 can be estimated by dividing these values of M_c by a repeating unit mass M₀= 270 g.mol⁻¹ (this value
 427 assumes that elastically active chains consist essentially of polymerized diOHC16 monomer units in which
 428 only 1 acid and 1 hydroxyl group have reacted.)

429 The values of the ratio M_c/M₀ calculated in **Table 2** suggest that for samples PG0.4, PG2.3 and PG3.9
 430 the number of polymerized diOHC16 repeating units should range from 5 to 7, while 19 to 21 repeating
 431 units are predicted for samples PG4.8, PG5.2 and PG6.2. For these latter, a few glycerol units are probably
 432 also present in the elastically active chains. Anyhow, such a loosening of the network induced by the
 433 gradual introduction of the glycerol is in full accordance with the increase in the labelling of free OH groups
 434 within the co-polyesters (**Figure 3**).

435 Besides, the plot of ν and M_c as a function of this molar content of glycerol chemically bound to the
 436 network is shown on Figure 5B. A sharp transition from dense amorphous networks (PG0.4, PG2.3 and
 437 PG3.9) to loose semi-crystalline networks (PG4.8, PG5.2 and PG6.2) seems to take place around a threshold
 438 value of 12 mol% of glycerol.

439 The development of a crystallinity for higher glycerol contents may be ascribed to the flexibility of
440 the long chain segments between two crosslinks which become able to fold into crystallites, while at lower
441 glycerol content the shorter chains remain amorphous.

442 According to the different chemical structures highlighted by the structural and thermal
443 characterization of the different co-polyesters, we further checked their tensile mechanical properties. The
444 determined tensile strength, strain at break and Young Modulus are reported on **Table1**, and the
445 characteristic curve are superimposed on the **Figure 6**.

446

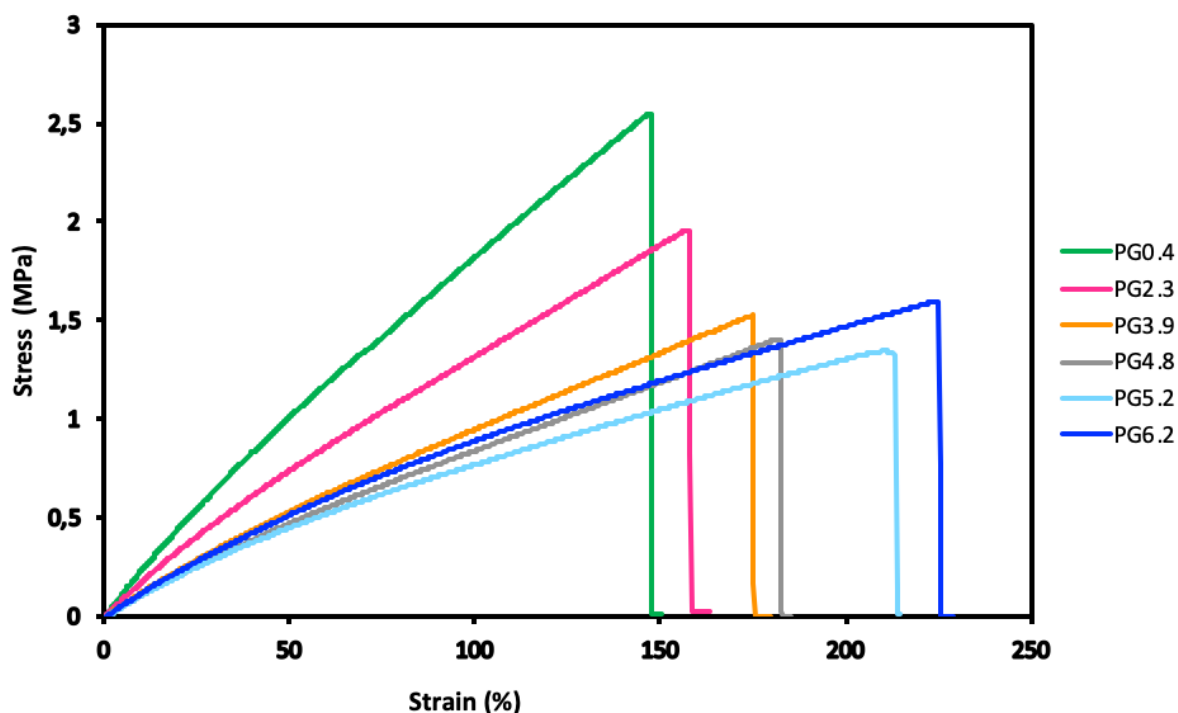


Figure 6- Typical Stress-strain curves of the cutin-like diOHC16-glycerol co-polyester films from 0.4 % wt. for PG0.4 to 6.2% wt. for PG6.2

447

448

449 All co-polyesters, either with low or high content of glycerol, show a quasi linear and reversible
450 stress-strain behavior that is characteristic of polyesters exhibiting rubber elasticity comparable to
451 synthetic elastomers. The mechanical properties of the PG0.4, were comparable to those previously

452 described with other polyhydroxylated fatty acids^{21, 24}. Moreover, our present data show that the
453 mechanical properties were strongly modified by the gradual introduction of glycerol in the co-polyesters
454 which resulted in a decrease in the Young modulus (from 2.29 to 1.19 MPa), as well as in the stress at
455 break (from 2.1 to 1.5 MPa). Surprisingly, higher glycerol of 6% induces a slight increase of tensile strength
456 simultaneous to the increase of strain at break. It is certainly due to the crystallinity evidenced by
457 calorimetry and XRD measurements (Figure 4).

458 The most striking observation is the increase in strain at break from 124% to 217 % (for PG0.4 and
459 PG6.2 respectively) induced by the esterified glycerol in the co-polyesters (**Table1, Figure 6**). This
460 elongation value is comparable to some synthetic rubber such as ethylene-propylene-diene or polysulfide-
461 butadiene rubbers²⁵. This strain at break induced by an higher glycerol/hydroxy-fatty acid ratio fully fits
462 the CUS1 tomato phenotype which is affected in cutin deposition¹¹. Importantly, the CUS1 tomato cutin
463 polyester exhibited a fivefold increase in the glycerol ratio (vs hydroxylated fatty acids), which probably
464 account for the increase in its extensibility and the absence of cracks observed on the CUS1 fruits,
465 regardless that their cuticle density shows a threefold reduction¹⁰.

466

467

468 **Glycerol can modify the barrier properties of the co-polyesters and their interaction with bacterial cells**

469 Water permeance and oxygen barrier properties of the co-polyesters were analyzed. All the produced co-
470 polyesters showed low water vapor permeance properties (**Figure 7A**) around $10^{-9} \text{ m}\cdot\text{s}^{-1}$, in the same range
471 than the plant cuticle permeance and some synthetic membrane, such as 3 μm parafilm or 3 μm
472 polyethylene²⁶. The introduction of esterified glycerol and the associated modification of the branching of
473 the co-polyesters induced a slight, but statistically not significant increase in the water vapor permeability
474 of the co-polyesters. This result is consistent with our previous data showing that a modification of the
475 polymerization index did not significantly impact the water permeance of tomato cutins (Philippe et al,
476 2016).

477

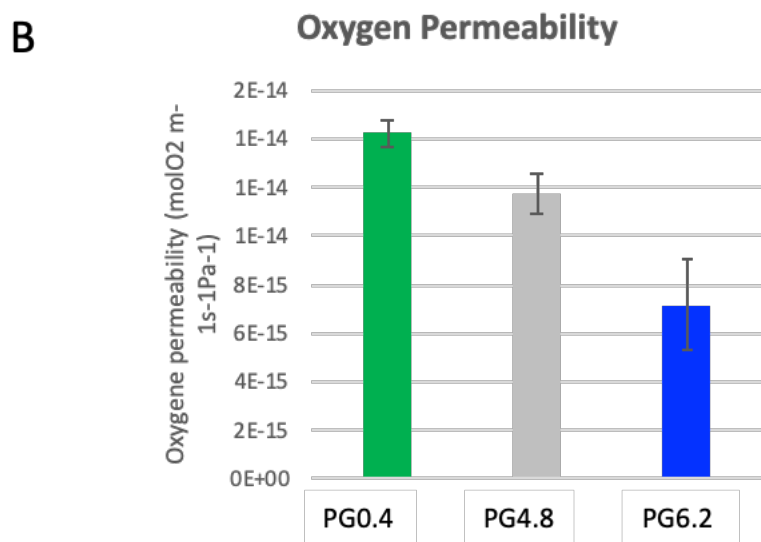
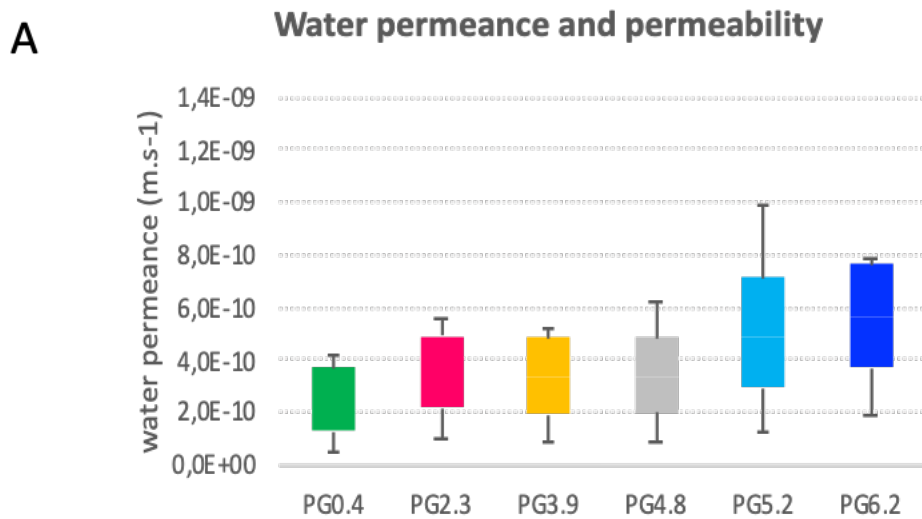


Figure 7- Barrier properties of the cutin-like co-polyesters

Water permeance (A) and Oxygen (B) barrier properties of the cutin-like diOHC16-glycerol co-polyesters containing increasing level of glycerol (0.4 %wt for PG0.4 to 6.2% wt for PG6.2)

478

479

480 The oxygen permeability of the cutin-derived co-polyesters ranged between 0.7 and 1.4 x 10⁻¹⁴ mol
 481 m⁻¹s⁻¹ Pa⁻¹ (Figure 7B). These values are in the same order of magnitude of synthetic polymers commonly
 482 used for food packaging such as low-density polyethylene (0.1-0.2 x 10⁻¹⁴ mol.m⁻¹.s⁻¹.Pa⁻¹)^{16, 27, 28}. These
 483 values are also comparable to polylactic acid (PLA), a bio-based polyester, for which oxygen permeability
 484 values ranging between 1x10⁻¹⁶ and 1x10⁻¹⁴ mol. m⁻¹.s⁻¹.Pa⁻¹ have been reported²⁹⁻³¹. Other polyesters such

485 as fossil-based polyethylene terephthalate, or microbial synthesized polyhydroxyalkanoates (PHAs) have
486 considerably higher barrier properties with oxygen permeability in the order of $1 \times 10^{-17} \text{ mol m}^{-1} \text{ s}^{-1} \text{ Pa}^{-1}$ ³²,
487 ³³.

488 Interestingly, increasing the ratio of esterified glycerol in the co-polyesters improved the films
489 oxygen barrier properties by reducing oxygen permeability by half (**Figure 7B**). This is probably associated
490 with the increase of crystallinity, as observed for other elastomers ³⁴ reducing the motion needed for
491 oxygen diffusion.

492 Finally, the antibacterial activity of the co-polyesters containing the lowest and the highest levels
493 of esterified glycerol (PG0.4 and PG6.2) was assessed on *E. coli* and *S. aureus*. After exposure to the co-
494 polyester films, no labelling of dead cells was revealed (**Figure 8A**), which indicates that the co-polyesters
495 were devoid of bactericidal properties regardless of the glycerol content. This result contrasts with the
496 biocide activity that was demonstrated with acyl glycerol esters of hydroxy-fatty acids ³⁵ or with films
497 formed by self-assembly of these esters ^{36, 37} extracted by an ionic liquid catalyst from suberin, another
498 hydrophobic plant polyesters.

499 Since the co-polyesters are devoid of bactericidal capacity, we further analyzed the films' surface
500 following their incubation with bacteria (**Figure 8 B**). For either co-polyester, the numbers of adherent *E.*
501 *coli* cells were low and comparable. Remarkably over the surface of the PG0.4 co-polyester, *S. aureus*
502 formed a compacted biofilm whereas PG6.2 hinder significantly the adhesion of this bacteria species. This
503 result demonstrates that increased glycerol levels in the cutin inspired co-polyesters leads to significant
504 reducing of bacterial fouling. (**Figure 8 B**). The observed differences between the two bacteria species
505 might be due to the electronegativity of the cells surface that is higher in *E. coli* than *S. aureus*, regardless
506 that their different morphologies and surface roughness (rods and cocci, respectively) may greatly
507 influence their adhesion in the conditions used here. This observation, supported by the structural, thermal
508 and mechanical analyses, suggests that glycerol esterification altered the smoothness of the films' surface
509 as well as their surface charge. One important finding is that by increasing further the glycerol levels in the
510 cutin co-polyesters their anti-biofouling properties can be potentiated.

511

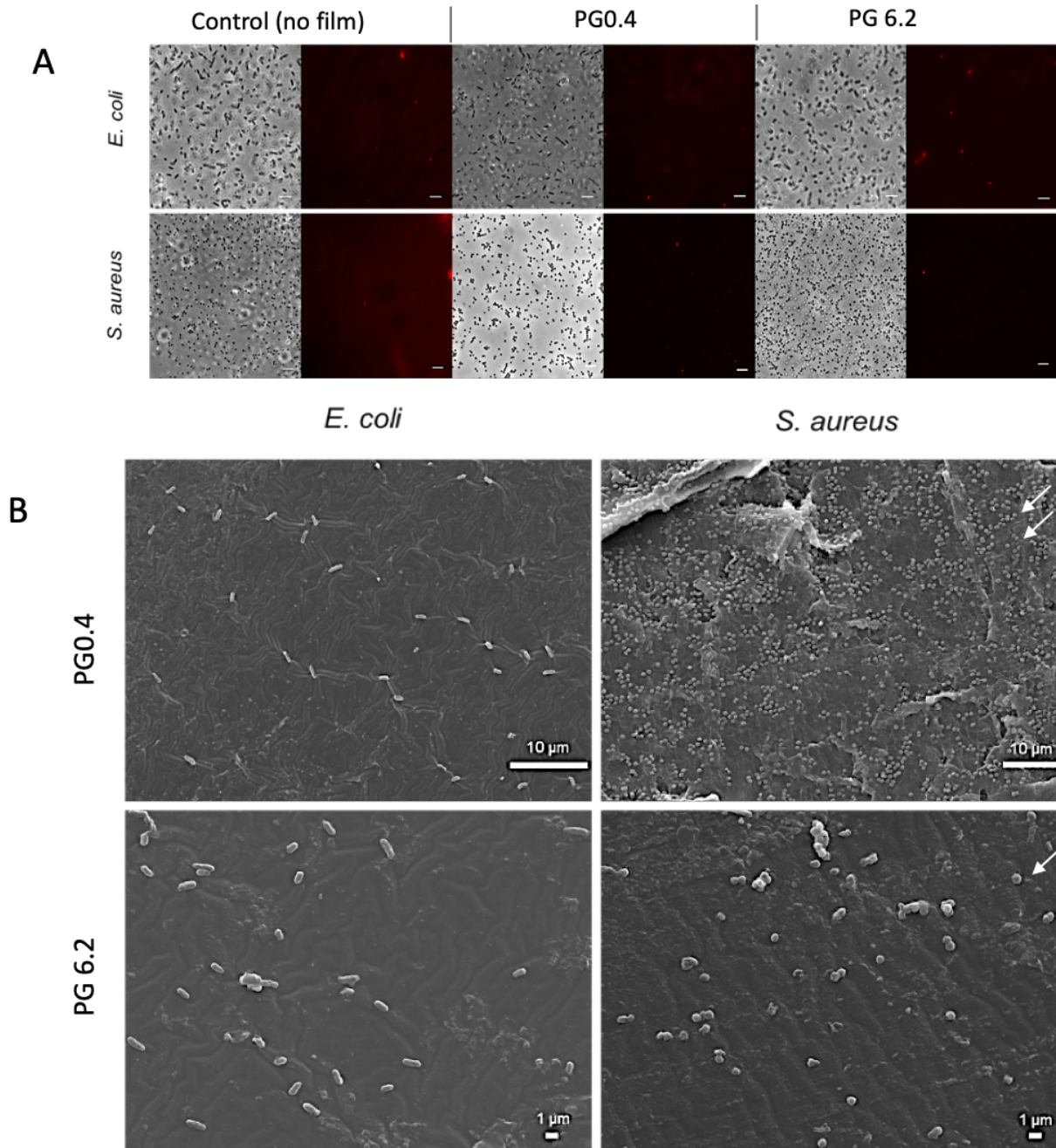


Figure 8. Microscopy imaging of the cutin-like co-polyesters PG0.4 and PG6.2 after incubation with *E. coli* and *S. aureus*.

A. Co-polyesters films activity against *E. coli* and *S. aureus*. Following exposure of bacteria to films pieces their morphology and viability were visualized by phase-contrast and fluorescence microscopy using Texas Red filter (dead cells are revealed by red fluorescence due to propidium iodide labelling), respectively. Controls was conducted without films. The scale bar in all images is 5 μ m.

B. Cells adherent onto the surface of the cutin co-polyester films were observed by SEM microscopy. No differences were noticed in the numbers of adherent *E. coli* cells in either co-polyester films. Conversely, the number of *S. aureus* adherent cells (ex under arrows) are significantly higher in the PG0.4 co-polyester compared to the PG6.2. The scale bar in all images is shown at the bottom.

513 **Conclusions**

514 We report in this work, the sustainable production of glycerol/hydroxy-fatty acid co-polyesters by
515 a catalyst- and solvent-free polycondensation process. Glycerol and hydroxy-fatty acids are biosourced
516 molecules from by-products and wastes produced by the oilseed and tomato processing industries,
517 respectively. The hydroxy-fatty acid fraction used in this work was prepared using an improved process
518 compared to what is done today on an industrial scale. Therefore, the production of these
519 glycerol/hydroxy-fatty acid co-polyesters meets the requirements of green chemistry and sustainability.
520 These co-polyesters are inspired from the cutin polymer of plant cuticles, which is also composed of
521 hydroxy-fatty acids and glycerol. Drawing on our previous studies on tomato fruit cuticle, we gradually
522 increased the glycerol content while remaining in a concentration range observed in most plant cuticles.
523 This biomimetic approach can be seen as a step forward in the production of natural elastomeric networks
524 which is a very active field for instance from natural rubber^{23, 38}. The produced co-polyesters displayed
525 good elastomers properties, quite comparable to those of some synthetic rubber polymers. By adjusting
526 the level of esterified glycerol, we induced modifications of the reticulation pattern which was associated
527 to variation in chain mobility and extensibility. Glycerol also induced the loosening of the co-polyester
528 network and the formation of crystalline domains. These modifications were associated to variations in
529 the mechanical and barrier properties of the co-polyesters as well as adhesion of microorganisms.

530 Actually, these hydroxy-fatty acid/glycerol co-polyesters provide excellent templates to further delineate
531 the relationships between the complex molecular and macromolecular architecture and the functional
532 properties of plant cuticular barriers, while developing green polymer composites adapted to specific
533 applications for food, packaging industry or as antifouling natural product. Furthermore, increasing
534 contents of glycerol led to available free hydroxyl groups for grafting and covalent substitutions for tailored
535 functionalization, opening new routes for high-value applications (e.g., in the medical sector).

536

537

538 **Acknowledgment**

539 This work was supported by INRAE Transfer grant (ELASTOMAT project) and the INRAE
540 TRANSFORM department. RR is grateful to FCT funding for his PhD scholarship (SFRH-BD-110467-2015).
541 The authors thank Mr André Lelion for his technical assistance.

542

543 **References**

544

545

546

547

548

549

550

551

552

553

554

555

556

557

558

559

560

561

562

563

564

565

566

567

568

569

570

571

572

573

574

575

576

577

578

579

580

581

582

583

584

585

586

587

588

589

1. Fich, E. A.; Segerson, N. A.; Rose, J. K., The plant polyester cutin: biosynthesis, structure, and biological roles. *Annu. Rev. Plant Biol.* **2016**, *67*, 207-233. <https://doi.org/10.1146/annurev-arplant-043015-111929>
2. Nawrath, C., Unraveling the complex network of cuticular structure and function. *Curr. Opin. Plant Biol.* **2006**, *9* (3), 281-287. <https://doi.org/10.1016/j.pbi.2006.03.001>
3. Yeats, T. H.; Rose, J. K., The formation and function of plant cuticles. *Plant Physiol.* **2013**, *163* (1), 5-20. <https://doi.org/10.1104/pp.113.222737>
4. Fameau, A.-L.; Gaillard, C.; Marion, D.; Bakan, B., Interfacial properties of functionalized assemblies of hydroxy-fatty acid salts isolated from fruit tomato peels. *Green Chem.* **2013**, *15* (2), 341-346. <https://doi.org/10.1039/C2GC36677K>
5. Heredia-Guerrero, J. A.; Heredia, A.; Dominguez, E.; Cingolani, R.; Bayer, I. S.; Athanassiou, A.; Benitez, J. J., Cutin from agro-waste as a raw material for the production of bioplastics. *J. Exp. Bot.* **2017**, *68* (19), 5401-5410. <https://doi.org/10.1093/jxb/erx272>
6. Fritsch, C.; Staebler, A.; Happel, A.; Cubero Márquez, M. A.; Aguiló-Aguayo, I.; Abadias, M.; Gallur, M.; Cigognini, I. M.; Montanari, A.; López, M. J.; Suárez-Estrella, F.; Brunton, N.; Luengo, E.; Sisti, L.; Ferri, M.; Belotti, G., Processing, valorization and application of bio-waste derived compounds from potato, tomato, olive and cereals: A Review. **2017**, *9* (8), 1492. <https://doi.org/doi:10.3390/su9081492>
7. Benítez, J. J.; Castillo, P. M.; Del Río, J. C.; León-Camacho, M.; Domínguez, E.; Heredia, A.; Guzmán-Puyol, S.; Athanassiou, A.; Heredia-Guerrero, J. A., Valorization of tomato processing by-products: fatty acid extraction and production of bio-based materials. *Materials (Basel)* **2018**, *11* (11). <https://doi.org/10.3390/ma11112211>
8. Quispe, C. A. G.; Coronado, C. J. R.; Carvalho Jr, J. A., Glycerol: production, consumption, prices, characterization and new trends in combustion. *Renew. Sust. Energ. Rev.* **2013**, *27*, 475-493. <https://doi.org/10.1016/j.rser.2013.06.017>
9. Graça, J.; Schreiber, L.; Rodrigues, J.; Pereira, H., Glycerol and glyceryl esters of omega-hydroxyacids in cutins. *Phytochemistry* **2002**, *61* (2), 205-215. [https://doi.org/10.1016/s0031-9422\(02\)00212-1](https://doi.org/10.1016/s0031-9422(02)00212-1)
10. Girard, A. L.; Mounet, F.; Lemaire-Chamley, M.; Gaillard, C.; Elmorjani, K.; Vivancos, J.; Runavot, J. L.; Quemener, B.; Petit, J.; Germain, V.; Rothan, C.; Marion, D.; Bakan, B., Tomato GDSSL1 is required for cutin deposition in the fruit cuticle. *Plant Cell* **2012**, *24* (7), 3119-34. <https://doi.org/10.1105/tpc.112.101055>
11. Philippe, G.; Gaillard, C.; Petit, J.; Geneix, N.; Dalgalarondo, M.; Bres, C.; Mauxion, J. P.; Franke, R.; Rothan, C.; Schreiber, L.; Marion, D.; Bakan, B., Ester cross-link profiling of the cutin polymer of Wild-Type and cutin synthase tomato mutants highlights different mechanisms of polymerization. *Plant Physiol.* **2016**, *170* (2), 807-20. <https://doi.org/10.1104/pp.15.01620>
12. Barker, J. C., Russeting (cuticle cracking) in glasshouse tomatoes in relation to fruit growth. *J. Hortic. Sci.* **1988**, *63* (3), 459-463. <https://doi.org/10.1080/14620316.1988.11515879>
13. Philippe, G.; Geneix, N.; Petit, J.; Guillon, F.; Sandt, C.; Rothan, C.; Lahaye, M.; Marion, D.; Bakan, B., Assembly of tomato fruit cuticles: a cross-talk between the cutin polyester and cell wall polysaccharides. *New Phytol.* **2020**, *226* (3), 809-822. <https://doi.org/10.1111/nph.16402>
14. Shen, Y.; Xu, Z., An improved GC-MS method in determining glycerol in different types of biological samples. *J. Chromatogr. B Analyt. Technol. Biomed. Life Sci.* **2013**, *930*, 36-40. <https://doi.org/10.1016/j.jchromb.2013.04.034>
15. Schreiber L; J, S. n., Water Permeability. In *Water and solute permeability of plant cuticles*, Springer Berlin Heidelberg: Berlin, Heidelberg, 2009; pp 61-123.

- 590 16. Motedayen, A. A.; Rezaeigolestani, M.; Guillaume, C.; Guillard, V.; Gontard, N., Gas barrier
591 enhancement of uncharged apolar polymeric films by self-assembling stratified nano-composite films.
592 *RSC Advances* **2019**, 9 (19), 10938-10947. <https://doi.org/10.1039/C9RA01109A>
- 593 17. Tedeschi, G.; Benitez, J. J.; Ceseracciu, L.; Dastmalchi, K.; Itin, B.; Stark, R. E.; Heredia, A.;
594 Athanassiou, A.; Heredia-Guerrero, J. A., Sustainable fabrication of plant cuticle-like packaging films from
595 tomato pomace agro-waste, beeswax, and alginate. *ACS Sustainable Chem. Eng.* **2018**, 6 (11), 14955-
596 14966. <https://doi.org/10.1021/acssuschemeng.8b03450>
- 597 18. Cogognigni, I.; Montanari, A.; de la Torre Carreras, R.; Cardoso Bernet Montserrat, G. Extraction
598 method of a polyester polymer or cutin from the wasted tomato peels and polyester polymer so extracted
599 WO/2015/028299, 2014.
- 600 19. Lu, Z.; Wang, J.; Gao, R.; Ye, F.; Zhao, G., Sustainable valorisation of tomato pomace: A
601 comprehensive review. *Trends Food Sci. Technol.* **2019**, 86, 172-
602 187. <https://doi.org/10.1016/j.tifs.2019.02.020>
- 603 20. Heredia-Guerrero, J. A.; Benítez, J. J.; Domínguez, E.; Bayer, I. S.; Cingolani, R.; Athanassiou,
604 A.; Heredia, A., Infrared and Raman spectroscopic features of plant cuticles: a review. *Front. Plant Sci.*
605 **2014**, 5, 305. <https://doi.org/10.3389/fpls.2014.00305>
- 606 21. Benitez, J. J.; Heredia-Guerrero, J. A.; Guzman-Puyol, S.; Barthel, M. J.; Dominguez, E.;
607 Heredia, A., Polyhydroxyester films obtained by non-catalyzed melt-polycondensation of natural occurring
608 fatty polyhydroxyacids. *Front. Mat.* **2015**, 2, 10. <https://doi.org/10.3389/fmats.2015.00059>
- 609 22. Flory, J. P., Elasticity of rubber. In *Principles of Polymer Chemistry*, Ithaca, N.Y. : Cornell
610 University Press ed.; 1953; Vol. 11.
- 611 23. Tran, T.-N.; Guyomard-Lack, A.; Cerclier, C.; Humbert, B.; Colomines, G.; Pilard, J.-F.;
612 Deterre, R.; Bideau, J.-L.; Leroy, E., Natural rubber-based ionogels. **2018**, 6 (3), 251--
613 258. <https://doi.org/doi:10.7569/JRM.2017.634174>
- 614 24. Benítez, J. J.; Heredia-Guerrero, J. A.; Guzmán-Puyol, S.; Domínguez, E.; Heredia, A., Long-
615 chain polyhydroxyesters from natural occurring aleuritic acid as potential material for food packaging. *Soft*
616 *Materials* **2015**, 13 (1), 5-11. <https://doi.org/10.1080/1539445X.2014.993476>
- 617 25. Shanks, R. A.; Kong, I., General purpose elastomers: structure, chemistry, physics and
618 performance. In *Advances in Elastomers I: Blends and Interpenetrating Networks*, Visakh, P. M.;
619 Thomas, S.; Chandra, A. K.; Mathew, A. P., Eds. Springer Berlin Heidelberg: Berlin, Heidelberg, 2013;
620 pp 11-45.
- 621 26. Valeska Zeisler-Diehl, V.; Migdal, B.; Schreiber, L., Quantitative characterization of cuticular
622 barrier properties: methods, requirements, and problems. *J. Exp. Bot.* **2017**, 68 (19), 5281-
623 5291. <https://doi.org/10.1093/jxb/erx282>
- 624 27. Durmuş, A.; Woo, M.; Kaşgöz, A.; Macosko, C. W.; Tsapatsis, M., Intercalated linear low density
625 polyethylene (LLDPE)/clay nanocomposites prepared with oxidized polyethylene as a new type
626 compatibilizer: Structural, mechanical and barrier properties. *Eur. Polym. J.* **2007**, 43 (9), 3737-
627 3749. <https://doi.org/10.1016/j.eurpolymj.2007.06.019>
- 628 28. Matar, C.; Gaucel, S.; Gontard, N.; Guilbert, S.; Guillard, V., Predicting shelf life gain of fresh
629 strawberries 'Charlotte cv' in modified atmosphere packaging. *Postharvest Biol. Technol.* **2018**, 142, 28-
630 38. <https://doi.org/10.1016/j.postharvbio.2018.03.002>
- 631 29. Lehermeier, H. J.; Dorgan, J. R.; Way, J. D., Gas permeation properties of poly(lactic acid). *J.*
632 *Membr. Sci.* **2001**, 190 (2), 243-251. [https://doi.org/10.1016/S0376-7388\(01\)00446-X](https://doi.org/10.1016/S0376-7388(01)00446-X)
- 633 30. Mahmoodi, A.; Ghodrati, S.; Khorasani, M., High-strength, low-permeable, and light-protective
634 nanocomposite films based on a hybrid nanopigment and biodegradable PLA for food packaging
635 applications. *ACS Omega* **2019**, 4 (12), 14947-14954. <https://doi.org/10.1021/acsomega.9b01731>
- 636 31. Palai, B.; Biswal, M.; Mohanty, S.; Nayak, S. K., In situ reactive compatibilization of polylactic
637 acid (PLA) and thermoplastic starch (TPS) blends; synthesis and evaluation of extrusion blown films
638 thereof. *Industrial Crops and Products* **2019**, 141, 111748. <https://doi.org/10.1016/j.indcrop.2019.111748>
- 639 32. Ambrosio-Martin, J.; Fabra, M. J.; López-Rubio, A.; Gorrasi, G.; Sorrentino, A.; Lagaron, J. M.,
640 Assessment of ball milling as a compounding technique to develop nanocomposites of poly(3-

641 hydroxybutyrate-co-3-hydroxyvalerate) and bacterial cellulose nanowhiskers. *J. Polym. Environ.* **2016**, 24
642 (3), 241-254. <https://doi.org/10.1007/s10924-016-0767-6>
643 33. Crétois, R.; Follain, N.; Dargent, E.; Soulestin, J.; Bourbigot, S.; Marais, S.; Lebrun, L.,
644 Microstructure and barrier properties of PHBV/organoclays bionanocomposites. *J. Membr. Sci.* **2014**,
645 467, 56-66. <https://doi.org/10.1016/j.memsci.2014.05.015>
646 34. Wang, Y.; Gupta, M.; Schiraldi, D. A., Oxygen permeability in thermoplastic polyurethanes. **2012**,
647 50 (10), 681-693. <https://doi.org/10.1002/polb.23053>
648 35. Correia, V. G.; Bento, A.; Pais, J.; Rodrigues, R.; Haliński, Ł. P.; Frydrych, M.; Greenhalgh, A.;
649 Stepnowski, P.; Vollrath, F.; King, A. W. T.; Silva Pereira, C., The molecular structure and
650 multifunctionality of the cryptic plant polymer suberin. *Materials Today Bio* **2020**, 5,
651 100039. <https://doi.org/10.1016/j.mtbio.2019.100039>
652 36. Ferreira, R.; Garcia, H.; Sousa, A. F.; Guerreiro, M.; Duarte, F. J. S.; Freire, C. S. R.;
653 Calhorda, M. J.; Silvestre, A. J. D.; Kunz, W.; Rebelo, L. P. N.; Silva Pereira, C., Unveiling the dual role
654 of the cholinium hexanoate ionic liquid as solvent and catalyst in suberin depolymerisation. *RSC*
655 *Advances* **2014**, 4 (6), 2993-3002. <https://doi.org/10.1039/C3RA45910A>
656 37. Garcia, H.; Ferreira, R.; Petkovic, M.; Ferguson, J. L.; Leitão, M. C.; Gunaratne, H. Q. N.;
657 Seddon, K. R.; Rebelo, L. P. N.; Silva Pereira, C., Dissolution of cork biopolymers in biocompatible ionic
658 liquids. *Green Chem.* **2010**, 12 (3), 367-369. <https://doi.org/10.1039/B922553F>
659 38. Tran, T. K. N.; Colomines, G.; Nourry, A.; Pilard, J.-F.; Deterre, R.; Leroy, E., Hydroxyl
660 telechelic natural rubber-based polyurethane: Influence of molecular weight on non-isothermal cure
661 kinetics. *Thermochim. Acta* **2015**, 620, 51-58. <https://doi.org/10.1016/j.tca.2015.10.006>
662
663
664

cutin monomers batch composition	%	(s.d.)
p-coumaric acid	1.8	(0.3)
16-hydroxy-hexadecanoic acid	2.7	(0.4)
16,9(10)-dihydroxyhexadecanoic acid	92.2	(2.3)
Hexadecane-1,16-dioic acid	0.4	(0.03)
7/8-hydroxy hexadecan-1,16-dioic acid	2.9	(1.2)

Supplemental Table 1 – Composition of the hydroxy-fatty acid fraction extracted from tomato cutin from industrial tomato peels

Value are means (standard deviation) of three experiments

665

666